Master's thesis:
Software development of Glasgow University's pulsar telescope

Emma Carli

April 2, 2020

Abstract

I have upgraded the data analysis pipeline of the Acre Road pulsar telescope (a $10\,\mathrm{m}^2$ effective area Yagi antenna) to current pulsar research standards. The year-long dataset of observations of PSR J0332+5434 that I use in this project is subject to strong radio frequency interference, which I have mostly removed with a stringent cleaning procedure. I then recovered the pulsar signal from below noise levels via folding with `PRESTO` [Ransom, 2011], taking into account pulse frequency variations in `TEMPO` [Hobbs and Edwards, 2012]. I have extracted 1051 pulse times of arrival, using the `FFTFIT` method [Taylor, 1993] in `PRESTO` with a four-component Gaussian template of PSR J0332+5434's pulse shape. I performed timing and pulsar parameter fitting in `PINT` [Luo et al., 2019]. I determined the pulsar frequency and position parameters accurately: $f = 1.39954153774 \pm 9.7 \times 10^{-10}$ Hz; $\dot{f} = -4.00890 \times 10^{-15} \pm 9.6 \times 10^{-19}\,\mathrm{Hz\,s^{-1}}$; Right Ascension = 03:32:59.36004193 $\pm 3.9 \times 10^{-7}$ deg and Declination = 54:34:43.2890116 $\pm 8.3 \times 10^{-6}$ deg. The characteristic age and magnetic field inferred from these parameters are consistent with values derived using data from other observatories. The error on the times of arrival and their signal-to-noise ratios are much improved with the updated pipeline; with a minimum error of 173.95 μs, and a largest folded SNR of 13.48. The total summed pulse profile of the year of observations is in line with published observations of PSR J0332+5434's pulse shape, and has improved residuals with respect to the previous pipeline's results.

Contents

1 Introduction

I have written this report for my Physics and Astronomy Master of Science final year project at the University of Glasgow, under the supervision of Prof. Graham Woan.

The aim of this project is to upgrade the data analysis pipeline of the Acre Road pulsar telescope to current pulsar research standards. The previous pipeline was custom written in MATLAB with many approximations.

The instrument is an array of four Yagi antennae with $10\,\mathrm{m}^2$ effective area, a 13 degree beam and a microsecond precision clock. It has a smaller collecting area, bandwidth, and timestamp precision than large-scale radio astronomy observatories. It is situated in a populated and obstructed area, and is thus subject to strong radio frequency interference. The test dataset used in the analysis presented below comprises 1051 4-hour observations of PSR J0332+5434 made between May 2017 and June 2018. The pulsar signal is below the noise levels of the time series and can only be extracted by careful processing.

In this project, I aim to recover the 'hidden' pulsar signal and time it with precision, to compute pulsar parameters and generate a summed pulse profile for the whole year of observations.

Sections 2 and 3.1 introduce pulsar astrophysics and instrumentation. To complete this project's aim, I start by implementing an updated, more stringent data cleaning routine that still preserves astrophysical information, in section 3.2. Then, I fold the pulsar observations in phase, taking into account the spin and orbit of the Earth along with the pulsar slowdown, in section 4.1. I further determine the pulse times of arrival and signal-to-noise ratios, using a 4-component Gaussian template of PSR J0332+5434's pulse shape in section 4.2. Finally, I fit the frequency and position pulsar parameters in 4.3 and generate a summed pulse profile in 4.4. The results are presented throughout the report and some additional parameters are computed in 4.5. The limitations of this study are discussed in section 5. Section 6 concludes this report. Acknowledgements and my Python data analysis pipeline are in appendices A and B, respectively.

2 Pulsar astrophysics

Neutron stars are formed in core-collapse supernovae from stars within the intermediate mass range 8 $M_\odot$ to 20 $M_\odot$ [Lyne and Graham-Smith, 2012, p.16]. When the star runs out of fusion fuel, its radiation pressure drops. Hydrostatic equilibrium is lost and the gravitational force takes over. The star's radius decreases but its angular momentum is conserved, leading to a great increase in rotation rate. This causes a large dynamo effect (circulating charges produce a current which in turns engenders a magnetic field), and the original magnetic field lines growing closer together – an intense magnetic field is generated. The star then squeezes its protons and electrons into neutrons, and stops shrinking as it reaches neutron degeneracy pressure. The outer layers of the stars rebound on this hard core, causing a supernova explosion. Equilibrium is restored and the remaining stellar core has evolved to a neutron star [Kippenhahn et al., 2012, Chapters 36,37].

Some neutron stars begin as pulsars, which are amongst the most extreme objects of the Universe. They undergo one revolution in usually less than a second. They are remarkably small and dense, approximately the mass of our Sun contained in a radius of ten kilometres - most of the original mass having been shed away in the supernova explosion [Lyne and Graham-Smith, 2012, p. 16]. Further, they emit strongly beamed radiation from the poles of their exceptionally intense magnetic field. If the Earth happens to be in the periodical sweeping path of the beam, this radiation can be observed as pulses. Some pulsars have a better ability in timekeeping than atomic clocks. Any variation in the timing of the pulses can be a useful source of astrophysical information: gravitational waves, companion stars, planets, and more can be inferred from small time differences [Lorimer and Kramer, 2005, Chapter 2].

2.1 Pulsar radio emission

In this project, I analyse the electromagnetic emission of one pulsar in the radio domain. The radiation mechanism can be understood with a simplified model from Goldreich and Julian [1969]. This approach is convenient as there are several gaps in pulsar theory, but it still encompasses many of the observed pulsar properties [Lorimer and Kramer, 2005, pp. 63-65].

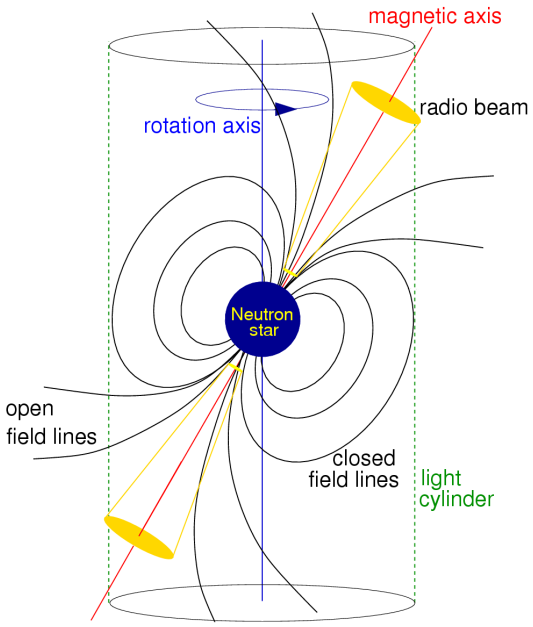

Figure 1: The simplified pulsar model adapted from [Lorimer and Kramer, 2005, p. 55].

In a pulsar's magnetosphere, there are free charges which co-rotate with the pulsar within the light cylinder (figure 1). At this limit, the plasma reaches the speed of light. This marks the border between closed and open field lines. At the pulsar's magnetic poles, where the open lines originate, there is a large electric field pulling the charges away from the surface. They are accelerated along these lines to relativistic energies and produce gamma-rays. This starts an avalanche of more charges and photons, which is proposed to result in the broadband coherent radio emission we detect, although the mechanism is not yet determined [Lorimer and Kramer, 2005, pp. 79-83]. This emission is very strongly beamed due to relativistic aberration and time compression, and the small emitting region [Lyne and Graham-Smith, 2012, pp. 247,253,254].

2.2 Slowdown of the pulses

Shortly after the first pulsar discovery in Hewish et al. [1968], Gold [1968] suggested that that the pulses should slow down. Indeed, the magnetic dipole moment of pulsars is not aligned with their rotation axis. In classical electromagnetism, this is commonly known to result in magnetic dipole radiation at the rotation frequency [Lorimer and Kramer, 2005, p. 60]. This emission is below the local plasma frequency, and gets absorbed before reaching us. This loss of energy results in the pulsar's rotational slowdown.

2.3 Frequency dispersion of the pulses

The radio emission of the pulsar propagates through the interstellar medium (ISM) to the observer. The refractive index of the ISM is frequency dependent, and thus, so is the travel time of the emission. The delay is usually expressed as:

$$\tau = 4.15 \cdot 10^3 \frac{1}{f^2} \mathrm{DM} \tag{1}$$

where τ is the delay induced by the ISM refraction in seconds, and f is the frequency of the radio wave in MHz. DM is the dispersion measure, which integrates the electron density of the ISM, n_e (cm^{-3}) on the travel path z (parsec), over the pulsar-observer distance, D parsec:

$$\mathrm{DM} = \int_0^\mathrm{D} n_\mathrm{e}(z) dz \tag{2}$$

Methods to remove this effect are discussed in section 3.1.1. It is a useful measure to probe the galactic densities. [Lorimer and Kramer, 2005, pp. 85,86]

2.4 Pulse shapes

Each pulse appears very different: the intensity is variable (sometimes nulled), the pulses can drift due to a rotating emission area, and the scintillation from the ISM and the atmosphere adds further modification [Lyne and Graham-Smith, 2012, Chapter 16]. Nevertheless, the average pulse profiles in each frequency band are stable, and are a unique identifier to each pulsar [Lyne and Graham-Smith, 2012, pp. 207,208].

The Acre Road pulsar telescope, the focus of this study, monitors the bright pulsar PSR J0332+5434. The 'J' prefix indicates 2000 coordinates, followed by the pulsar's right ascension and declination. Alternatively, in 1950 'B' coordinates, the pulsar is named PSR B0329+54. It was first detected in Cambridge, a year after pulsars were discovered [Cole and Pilkington, 1968]. It has a spin period of $\approx 0.714\,\mathrm{s}$. I am using the Jodrell Bank Observatory's template of its average pulse shape [Gould and Lyne, 1998]. This shape is very stable. However, it must be considered that this shape exhibits mode switching (i.e. it switches between two defined shapes), and the pulse's exact shape is debatable - 3 to 6 added Gaussians are proposed to approximate the shape [Kwofie, 2018, offers a good review].

3 Observations and data preparation

3.1 Pulsar telescopes

3.1.1 General design

The faint signal of pulsars is detected with large area radio receptors, usually dishes. Generally, the instrument observes over a wide bandwidth of one or two orthogonal polarisations, which is translated to voltage in a dipole. This voltage goes through low-noise amplifying and bandpass filtering. The signal is often heterodyned to baseband; i.e. the bandwidth is shifted to a zero centre frequency - the true centre can be added on later. This makes the lower-frequency signal easier to manage in circuits and processing [Lorimer and Kramer, 2005, p. 108]. The voltage is then squared (this is called detection), and thus converted to power. The timestamps of the data are usually provided by maser clocks [Bhattacharya, 1998].

Dispersion (introduced in section 2.3) spreads in time the broadband radio pulse into its frequency components, with the highest arriving first (figure 2). To restore the pulse's original shorter time span and higher brightness, dispersion must be removed. This can be done post detection, by dividing the bandwidth into small

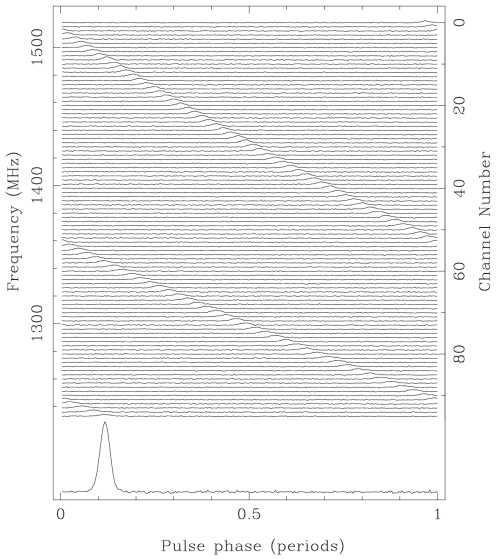

Figure 2: Pulse dispersion through frequency channels. The sharp, bright bottom pulse is dedispersed [Lorimer and Kramer, 2005, p. 20].

channels, and introducing delays corresponding to the pulsar's dispersion measure in each (equation 1). This method for incoherent dedispersion is called a (hardware or software) filterbank. It is limited in precision to the chosen width of the sub-bands, which are also dispersed [Lyne and Graham-Smith, 2012, pp. 37,38]. A more precise, yet more computationally intensive, method was introduced in Hankins [1971]: coherent dedispersion. It aims at exactly inverting the effect of the ISM by convolution with an inverse chirp at the required dispersion measure. This is done by performing a Fourier Transform (FT) on the data, adding phase delays corresponding

to each frequency, and transforming back to the time domain. This method happening pre-detection, the signal must then be squared.

3.1.2 The Acre Road pulsar telescope

The instrument at the focus of this study is an array of four high-gain Yagi antennae, sensitive to 407.5±2 MHz. It is located in Glasgow University's Acre Road Observatory, Glasgow, Scotland. It is driven in right ascension, with an effective area of about $10\,\mathrm{m}^2$ (figure 3). The observation beam diameter of this antenna can be worked out [Condon and Ransom, 2016, Section 3.1.4]:

$$\text{observed solid angle} = \frac{\text{observed wavelength}^2}{\text{effective area}} \tag{3}$$

and

$$\text{observed beam angular diameter} \simeq \sqrt{\text{observed solid angle}} \simeq 13 \text{ degrees} \tag{4}$$

It has been used to compile a dataset of several years of tracking the pulsar PSR J0332+5434 of one linear polarisation of electromagnetic (radio) waves. A Python code executes the driving, which goes on at regular intervals rather than continuously to reduce noise from the electronics. The radio receiver is software defined [Ettus Research, GNURadio]. The timestamps are made with a GPS disciplined temperature-controlled crystal oscillator [Trimble], using a UTC (Universal Time Coordinated) timescale. The voltage is increased by low-noise amplifiers. Coherent dedispersion is performed on the voltage by the `simple_ra` software [Leech]. The squared signal is bandpass filtered, downsampled to 2 ms, and saved to disk. The GPS time of the start of the observation is written in the filename, with a resolution of 1 microsecond. I show in sections 4.2 and 4.3 that this hard limit is well below other sources of error, and thus virtually does not affect the analysis.

This is similar to the standard systems described in 3.1.1 above, with a smaller collecting area, bandwidth, and timestamp precision.

Figure 3: Computer model of the Acre Road pulsar telescope [Perreur-Loyd, 2003].

3.2 The data

3.2.1 Data characteristics

The dataset used in this project is formed of just over a year (May 2017 to June 2018) of 4-hour observations of PSR J0332+5434, 1051 in total. These were the only raw files available. This choice is not too restrictive, as there are software and hardware changes that impacted observations prior to this period. For the previous three years of observations, only files cleaned with the previous routine were kept.

The data, a time series of detected power, is written in 4-byte (32 bits) single precision floating point numbers. It is subject to much more Radio Frequency Interference (RFI) than large-scale radio astronomy observatories. Indeed, the instrument is situated in a populated area. Some buildings and vegetation obstruct the sky. In addition, the antenna beam pattern has sidelobes observing the ground. Even weak sources of RFI

are detected, since the gain of the front end amplifier is about 80 dB. The amplifier also contributes to the noise levels.

Ideally, the observations should look like white noise overlaid with PSR J0332+5434's pulses, as appears in figure 2. However, the Acre Road observations have a low signal-to-noise ratio (instantaneous SNR < 1), and thus the pulses are 'buried' in the noise. It is this project's aim to uncover them. The noise is a blend of several recurring features:

- A gradual "bump" in standard deviation and/or mean (increase and decrease). This is due to the telescope's path passing through a radio source like the Sun, the Moon, a building, a tree, etc.;
- A transitory increase in the mean (simple sinusoid RFI which increases the power level) and/or standard deviation;
- Impulsive interference: very short, sudden jumps in the data;
- Noise due to the driving of the telescope. This appears every 10 minutes. The drive is on for less than 30 seconds and generates noise at high power. Subsequently, when the beam has been displaced, there is a change in mean. This is due to a different portion of the sky (e.g. galactic plane) and the premises coming inside the beam.

The features listed here are visible in figure 4.

3.2.2 Data cleaning

To mitigate the negative impact of RFI on the observations, I remove large changes which do not come from the weak pulsar emission. Throughout, I use a median function, which is more robust to outliers than a mean. I have implemented the data cleaning routine as follows, in order:

1. Cropping the data to an integer number of minutes, to be able to operate on minute or second-long blocks;
2. Removing the median of the dataset as a whole;
3. Removing a median from each one-second block. The duration of these blocks was chosen to be longer than the pulsar's period, but short enough to capture variability. This removes power level changes;
4. 5 sigma clipping with a median centre function over one minute blocks. This removes impulsive interference (including the driving);
5. Whitening the signal by dividing each one minute block by its standard deviation.

Step 3 replaces a median filter to reduce computation time. The data is divided into consecutive blocks. Therefore, unlike a filter, this method will leave median steps every minute. Upon close inspection of several datasets, it appears these steps are minimal. The duration of the blocks in step 4 was chosen to be more than twice a driving period, but short enough so that large, sudden standard deviation changes are not 'cropped'. This means that impulsive interference that lasts a significant part of a minute will contribute to the median and will not be completely clipped. I made this choice since cutting data with a large standard deviation is an information loss, whereas not clipping a short noise impulse is not. The sigma clipping must be performed before whitening to obtain good standard deviation estimates. My Python implementation is shown in appendix B.

The previous routine's main difference is that it clipped outliers with a fixed, very high power level (bad), but it used a median filter (good). Whitening was done while folding. I have not tested whether using the previous routine's cleaning would better or worsen the analysis, as it would take very long to run. Visually, the pre-whitening observations look much cleaner, i.e. more like white noise. An example of a cleaned dataset can be seen in figure 4.

After cleaning, I performed an average of each dataset's Fast Fourier Transforms (FFT), to visualise at what frequencies noise usually appeared. It shows strong features throughout: see figure 5.

PSR J0332+5434 has a frequency of about 1.4 Hz. On the Fourier transform, no strong features appear at this frequency and its harmonics, which shows the dominance of RFI on the dataset even on cleaned files. A small peak (compared to other RFI) appears at the frequency of the telescope drive (every 10 minutes, not shown on figure). This underlines that the power introduced by the driving of the antenna is not significant.

There also exists data cleaning routines in the pulsar software packages `PSRCHIVE` [Hotan et al., 2004] and `PRESTO` [Ransom, 2011]. These make use of dispersion as a good discriminator to distinguish pulsars from RFI. This is not applicable on the available data from the Acre Road telescope since it is not divided into frequency channels, and the data is de-dispersed before it is recorded.

I will show the cleaning's positive impact on the analysis in sections 4.2.2 and 4.4.

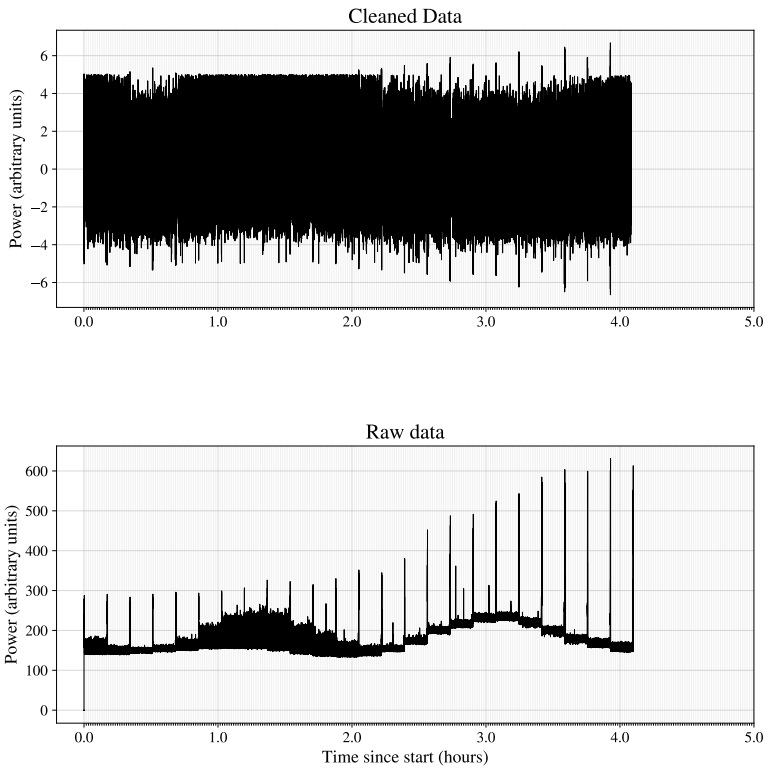

Figure 4: Data cleaning. Standard deviation and mean changes are almost entirely removed, with the exception of some residual drive jump power. The features listed in section 3.2.1 are visible: a radio source crossing (gradual bump in standard deviation), impulsive interference every ten minutes due to the telescope drive turning on (large spikes), and step changes in the mean after telescope displacement (different portion of the sky and premises coming into the beam).

4 Data analysis

4.1 Folding

In section 3.2.1, I have mentioned that the pulsar signal is hidden below noise levels and that this project's aim is to uncover this signal. This is done through a process called folding.

4.1.1 Introduction

Pulsar monitoring programmes, like the one undertaken at Acre Road, are designed for pulsar timing. This is the process of timing the pulses with extreme precision.

In some large telescopes, the time of arrival (TOA) of individual pulses can be retrieved directly from the data, like in figure 2. But in many cases, the Acre Road telescope included, the instantaneous SNR is too low to do this. To improve the signal, a group of pulses is adequately added on a chosen pulse. This is the process of folding. The TOA of the said pulse can then be determined, as the folded power time series pulse profile has a much higher folded SNR. I chose to fold each 4-hour observation entirely, as it was done previously, for comparison. This allows a reasonable folded SNR (over 6, see section 4.2.2).

If the interval of time between each pulse was the same, the data could be easily divided into period-long blocks and the latter added together. Nevertheless, there are processes that cause the emitted and received pulse intervals to vary. I take into account two effects affecting variably the observed period of the pulsar: Doppler shifts due to the relative velocity to the pulsar (rotation of the Earth on its own axis and around the Sun) ; and a smaller effect, the pulsar's slowdown (introduced in section 2.2). These effects are **not removed**, but simply computed to align the pulses correctly.

One must consider the phase of the pulses to align them for folding. The common method is to create an

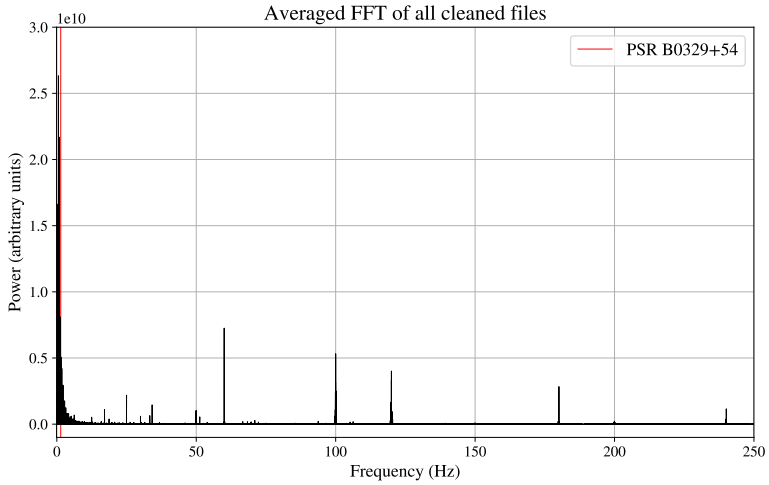

(a) Strong RFI power peaks appear at multiples (harmonics) of 60 Hz and at 100 Hz.

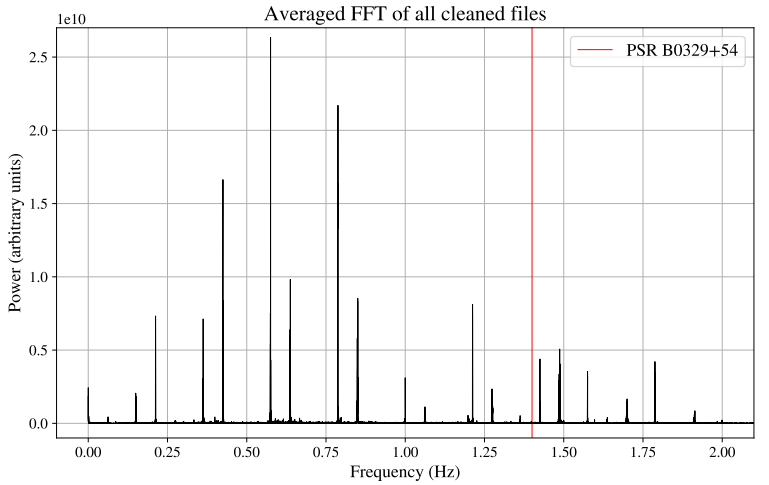

(b) A zoom on the lower frequency components of the RFI. The strongest frequency of power variation overall is at $\simeq$ 0.575 Hz – a period of $\simeq$ 1.74 seconds.

Figure 5: The averaged Fast Fourier Transform of cleaned files, which shows frequencies at which interference is strongest. It is important to note that the frequency of power variations is plotted, and not the electromagnetic (EM) frequency. The EM frequencies of the radio waves received are all assigned to one channel (407.5±2 MHz).

array of bins, each of which corresponds to a pulse phase, given by [Condon and Ransom, 2016, Chapter 6]:

$$\frac{\mathrm{d}\phi}{\mathrm{d}t} = f \tag{5}$$

or, in a Taylor expansion polynomial approximation,

$$\phi(t) = \phi(\mathrm{t}_0) + f(t - \mathrm{t}_0) + \frac{1}{2}\dot{f}(t - \mathrm{t}_0)^2 \tag{6}$$

Where ϕ, the phase, is a dimensionless number between 0 and 1, which measures the turn of the pulsar between 0 and 2π radians; t_0 is a chosen reference time, usually of zero phase, and f is the instantaneous pulse frequency at the observatory (i.e. **topocentric** frequency). The point of 0 phase is taken to be the pulse. f is the variable that needs computed regularly due to varying Doppler shifts and the pulsar slowdown, to attribute the correct phase to a datapoint.

4.1.2 Pulsar topocentric frequency predictions

The 4-hour observations' datapoints must be distributed in their correct pulsar phase bin. To do so, I must calculate equation 6, a polynomial approximation of the phase, for each block.

For each datapoint, time can be worked out using the GPS timestamp (UTC timescale) of the start of the observation and the instrument's sampling frequency (2 ms). It is very important that the GPS timestamp precision is kept in all conversions, to not introduce timing errors. In pulsar software, the time format is usually MJD with a UTC timescale. I made the conversion of start time from GPS to MJD (both UTC timescale) using the Python package `astropy`, enforcing microsecond precision (see appendix B).

I computed t_0, $\phi(t_0)$ and a polynomial approximation of the evolution of f for each 4-hour observation using `TEMPO`, a pulsar timing software [Hobbs and Edwards, 2012]. To do so, known pulsar parameters must be input. They are shown in table 1.

Name	J0332+5434	Right Ascension	$03{:}32{:}59.4096 \pm 1.000 \times 10^{-4}$ deg
Declination	$+54{:}34{:}43.329 \pm 1.000 \times 10^{-3}$ deg	f	$1.399541538720 \pm 6.000 \times 10^{-12}$ Hz
$\dot{f}$	$-4.011970 \times 10^{-15} \pm 1.400 \times 10^{-20}$ Hz s^{-1}	Frequency and position epoch (MJD)	46473.00
Dispersion Measure	0 cm^{-2}	Observing site	Acre Road Observatory

Table 1: The initial parameters input in `TEMPO` for computation of the evolution of the topocentric observed instantaneous pulsar frequency in equation 6. These were obtained from the ATNF Pulsar Catalogue [Manchester et al., 2005], which collected the positional data from Deller et al. [2018] and the frequency data from Hobbs et al. [2004].

The parameters in table 1 are necessary for `TEMPO` to compute the varying Doppler time delays in the direction of the pulsar from Acre Road which alter the observed frequency. The spindown of the pulsar is also computed.

On a Linux system with a `TEMPO` installation, for each observation, I performed these calculations by running in a terminal

```
tempo -ZOBS=AR -ZFREQ=407.5 -ZTOBS=4 -ZSTART=<start of observation MJD> -ZSPAN=4H -f
    ↪ J0332+5434_initial_parameters.par
```

Listing 1: The `TEMPO` command. The automation of this command for each dataset is done in Python - see appendix B.

Where `AR` is the location of the Acre Road observatory, input in `TEMPO`'s observatory database (`obsys.dat`). `-ZTOBS` and `-ZSPAN` are the observation length and the time span covered by the polynomial coefficients, respectively. The `.par` file contains the parameters in table 1. I used the default number of polynomial coefficients but this can be changed using the option `-ZNCOEFF`.

The software outputs a file, called a 'polyco' or 'predictor' file, that contains the polynomial coefficients to model the evolution of the observed topocentric frequency, along with the observation parameters, the Doppler shift, and the reference (zero) phase and frequency.

Note that there are newer pulsar timing software: `TEMPO2` [Hobbs et al., 2006, Edwards et al., 2006] and `PINT` [Luo et al., 2019]. `PINT` is written in Python, as is this project, and hence I was planning to use it. Upon usage, however, I discovered a bug in the polynomial approximations. I have raised the issue to the `PINT` team which are now working on fixing it. I have used `TEMPO` rather than `TEMPO2` as it facilitated the compatibility with the folding software `PRESTO`. The corrections improvements in the newer version only apply to the most stringent standards of pulsar timing.

The previous routine in place at the Acre Road pulsar telescope did not employ standard software, but rather an approximation. It used a LIGO routine to compute the frequency of PSR J0332+5434at discrete times, which was linearly interpolated. $\dot{f}$ was simply calculated using adjacent frequencies. My approach is much more precise and easier to maintain.

4.1.3 Folding implementation

I used the pulsar searching software `PRESTO` [Ransom, 2011] to distribute the data into phase bins using the `TEMPO` predictions. On a Linux system with a `PRESTO` installation, for each observation, I ran in a terminal the following command:

```
prepfold -nosearch -polycos polyco.dat -psr 0332+5434 -double -noxwin -n 512 -o <path to
    ↪ the resulting folded pulse profile> <path to the cleaned observation datafile>
```

Listing 2: The `PRESTO` folding command. The automation of this command for each dataset is done in Python - see Appendix B.

Here, the option 'no search' is selected. I am indeed not aiming to search for this pulsar, but fold its observations using known quantities. `polyco.dat` is the output from command 1. I set the number of phase bins with the `-n` option. `-double` indicates that the input data consists of binary floats, while `-noxwin` removes any output windows (which is useful, as 1051 datasets are folded this way). Note that `PRESTO` will look for a `.inf` information file with the same path and name as the cleaned observation datafile. This file contains all the observation parameters: telescope name, bandwidth, channels, and beam diameter; pulsar name, dispersion measure and position; number of bins, sampling period, and interruptions in the observed time series. Not all this information is essential to the analysis I perform, but I have completed it for each datafile, to easily implement further `PRESTO` commands - see appendix B.

Note that the data is distributed in the bins without weighting by standard deviation in `PRESTO` [Scott Ransom, e-mail communication], and this is why I have performed the whitening in section 3.2.2 (data with a large standard deviation is more noisy and should be downweighted).

An example output of `PRESTO`'s `prepfold` command is shown in figure 12. Note that this particular plot has been produced with a different command, explained in section 4.3.2.

The softwares `SIGPROC` and `DSPSR` also offer folding routines [Lorimer, 2011, van Straten and Bailes, 2010]. The previous folding routine did not make use of these standard research tools, but an explicit MATLAB script. I will show in section 4.2.2 that using a research-standard pulsar folding software greatly improved the quality of the summed pulse profiles.

4.2 Time of Arrival and folded SNR computation

4.2.1 Introduction

Once the folded pulse profiles were formed, I had enough SNR to determine precisely the time of arrival of the pulse which was folded on (`PRESTO` chooses the time of arrival (TOA) of a pulse near the middle of the observation).

A first intuition may suggest defining the TOA as the maximum of the summed pulse profile. The latter being binned, this is not precise. Instead, a template pulse profile is usually needed. I obtained PSR J0332+5434's from the EPN Database of Pulsar Profiles - it is plotted in figure 6. It was observed for about an hour, at 408 MHz (which is in our observing frequency) by the 76 m Lovell Telescope at Jodrell Bank, England in several observations between 1987 and 1991 [Gould and Lyne, 1998].

There are several approaches to determine TOAs. Two accepted methods are [Hotan et al., 2004]:

- The `FFTFIT` method: It was introduced in Taylor [1993] and is the widely accepted method. It makes use of the 'shift theorem'. The analysed pulse profile being a time-shifted version of the template with added random noise, their relationship in the frequency domain is also simple. In a Fourier domain convolution of the analysed and template pulse profiles, the shift appears as a linear ramp which is least-squares fitted. It is very precise for high SNR profiles.

- Gaussian Interpolation Shift, Hotan et al. [2005]: the template and analysed pulse profiles are cross-correlated in the time domain. The cross-correlation function is fitted with a Gaussian, which allows interpolation between phase bins. The maximum of the Gaussian corresponds to the TOA. This is proposed as a better method when the SNR of the analysed pulse profile is low.

`PSRCHIVE` offer both methods. The software previously employed in the Acre Road pulsar telescope is a MATLAB script similar to the Gaussian Interpolation Shift method. I use `PRESTO`, which uses the `FFTFIT` method, for easy compatibility with the folds.

At this point of the analysis, the SNR of each folded pulse profile can be determined. To do so, the mean $\mu_{\text{off-pulse}}$ and standard deviation $\sigma_{\text{off-pulse}}$ of the off-pulse data must be computed. If a_i is the amplitude in phase bin i, the SNR is given by:

$$\text{SNR} = \frac{1}{\sigma_{\text{off-pulse}}\sqrt{\text{W}_{\text{eq}}}} \sum_{i}^{n_{\text{bins}}} (a_i - \mu_{\text{off-pulse}}) \tag{7}$$

where W_{eq} is the equivalent width of the pulse, i.e. the width in phase bins of a top hat pulse with the same area and peak height, or equivalently the pulse area divided by peak height [Lorimer and Kramer, 2005, p. 167]. The error on the time of arrival can thus be determined: it is the ratio of pulse equivalent width to SNR [Lorimer and Kramer, 2005, p. 202].

4.2.2 Implementation and results

I have mentioned in section 3.1.2 that the Acre Road instrument observes one polarisation: it is $\langle {E_y}^2 \rangle$, i.e. the expectation value of the square of the y polarisation of the electric field. The Jodrell Bank template is expressed

in terms of Stokes parameters, and I formed the template for the observed polarisation using formulae from Woan [2000]:

$$I = \langle {E_x}^2 \rangle + \langle {E_y}^2 \rangle$$
$$Q = \langle {E_x}^2 \rangle - \langle {E_y}^2 \rangle$$
$$\Rightarrow 2 \langle {E_y}^2 \rangle = I - Q$$

where I and Q are Stokes parameters. I fitted the $(I-Q)$ template pulse profile with four Gaussian components [Kwofie, 2018, figure 4.1] using `PRESTO`'s program `pygaussfit.py`, as shown in figure 6. This is less precise than using the original template to perform the `FFTFIT`. However, in `PRESTO`, this is not yet implemented - only observations folded with `PRESTO` or a n-Gaussian fit can be used as a template.

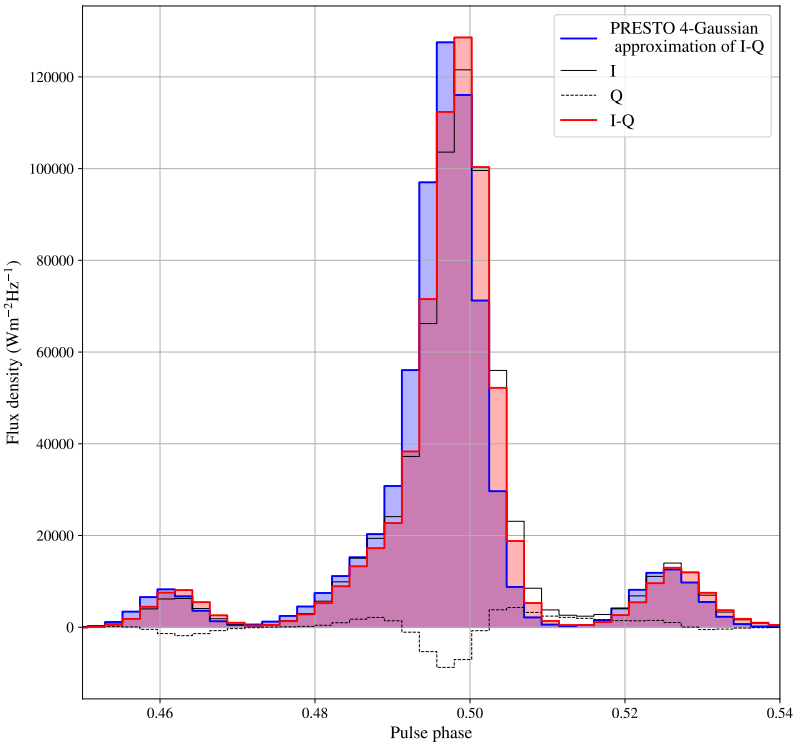

Figure 6: The I and Q Stokes parameters from the template pulse profile [Gould and Lyne, 1998], along with the $\langle {E_y}^2 \rangle$ observed polarisation $(I-Q)$. The Gaussian fit performed by `PRESTO`'s `pygaussfit.py` is also shown. It is close but not perfect.

I computed the TOA of each folded pulse profile by running the `PRESTO` command:

```
get_TOAs.py -f -n 1 -g <path_to_template_profile> <path_to_folded_profile>
```

Listing 3: The `PRESTO` TOA finding command. The automation of this command for each dataset is done in Python - see Appendix B.

The `-f` flag prompts the return of the calculated `FFTFIT` folded SNR with error. `-n` refers to the number of TOAs that one wants to extract from the folded pulse profile. `-g` indicates a Gaussian template.

I extracted 1051 TOAs from each 4-hour observation between May 2017 and June 2018, with an average error of 436.5 μs and a mean folded SNR of 6.63. Note that this is the very final result, after running the entire procedure detailed in the subsequent sections.

The previous method in place at Acre Road used interpolation of a convolution for TOA finding, as mentioned in 4.2.1. The SNR was simply calculated as the ratio of the time series' maximum with minimum subtracted over its standard deviation, and the TOA error as the ratio of the sampling period to SNR. This is an underestimate of the actual TOA error as all the folded pulses were wider than a bin (recall from 4.2.1 that the TOA error is the ratio of pulse equivalent width to SNR).

The previous method had extracted 3559 TOAs from observations spanning April 2014 to June 2018. Over the same period as my analysis (May 2017 to June 2018), the average SNR was just under 5. The highest folded SNR was under 9, while mine is 13.48.

The average TOA error, for folded pulse profiles with a SNR higher than 4, was approximately 342 μs (pulse width reduced underestimate). Other TOAs were not kept - the actual average of all the TOAs' error bars was greater. Applying a folded SNR cutoff of 4 for comparison, my average TOA error bar is at 349.58 μs. My lowest error on TOA is 173.95 μs, while the previous analysis' was $\simeq$ 236 μs.

It is clear that the new method I implemented has greatly improved scientific accuracy, and the results. Note that without data cleaning, the average folded SNR decreases by two, and the TOA error bars double.

The folded SNR's evolution in time is shown in figure 7, while the correlation between folded SNR and TOA error is shown in 8.

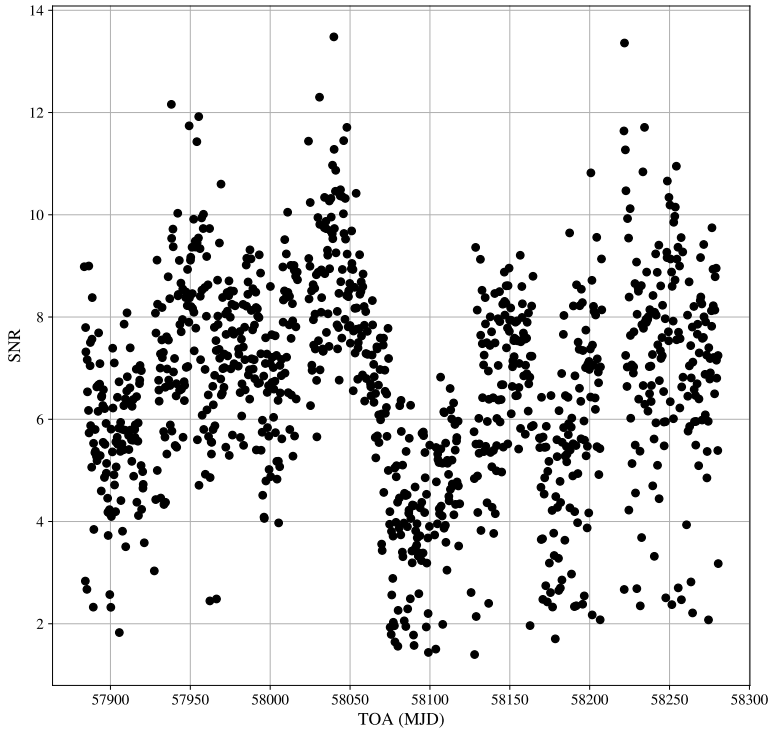

Figure 7: The evolution of SNR for folded 4-hour observation TOAs. Note that between MJD 58050 and 58100, there is a sharp decrease in SNR. This could be due to the telescope moving slightly off axis.

4.3 Timing fit

4.3.1 Timing

As explained in section 4.1.2, the start time of the observation was converted from GPS to MJD (UTC timescales) with microsecond precision in `astropy`. The TOAs were then calculated using the start time of the observation summed with the number of sample periods until the arrival. For pulsar timing, it does not matter that most pulses are missed out - solely that an integer number of pulsar rotations separates each TOA.

Recall that varying frequency Doppler shifts due to the Earth's motion and the pulsar slowdown were taken into account to align pulses, but not removed. The TOAs are thus topocentric, i.e. they are measured in the observatory reference frame. They must be converted to a standard inertial frame, so that the scientific results extracted from the TOAs are consistent with publications. In pulsar astronomy, this standard frame is the barycentre of the Solar System (SSB), i.e. its centre of mass [Stairs, 2002]. As mentioned in 4.1.2, there are several pulsar timing softwares used in research. To transform to this inertial frame, I used `PINT` [Luo et al., 2019] (for easy integration in my Python code).

The corrections performed to the TOAs are summarised below [Edwards et al., 2006, Hobbs et al., 2006, Stairs, 2002].

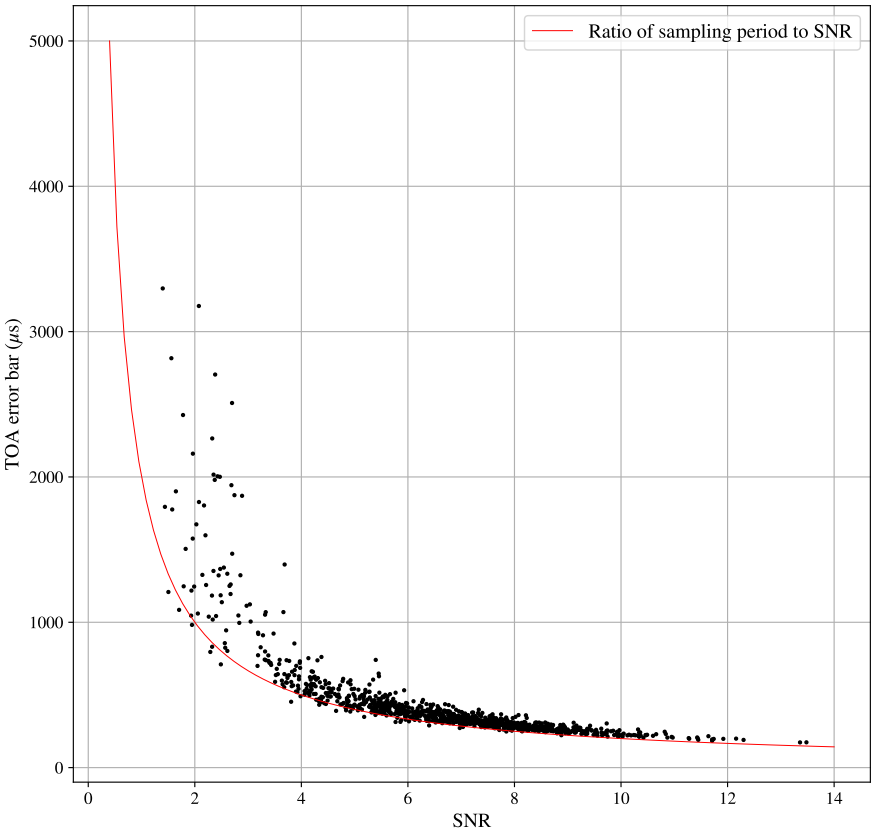

Figure 8: The TOA error bars with respect to the SNR of the corresponding folded observation. Recall that the TOA error is the ratio of equivalent pulse width to SNR (4.2.1). I have plotted the minimum TOA error with respect to SNR: one where the pulse width is one sampling period. As expected, the distribution is offset above this line. Below SNR 4, the points begin departing strongly from this ideal line - the folded pulse profiles are becoming quite wide, and the error bars on the TOAs grow sharply.

- The change in distance between the pulsar and the Earth as the latter goes around its orbit (called the Roemer delay);
- The gravitational redshift and time dilation undergone by the emission on its way to Earth, due to the Solar System (Einstein delay);
- The delays introduced by light going through stretched spacetime near the Solar System bodies (Shapiro delay);
- Clock corrections, a complex process that converts time as measured in the observatory to one in the inertial SSB frame (full explanation);
- Delays due to propagation in non-vacuum media, such as the atmosphere and the interplanetary medium;
- Doppler shifts due to Earth spin and orbit;
- The pulsar's proper motion and parallax.

To do this, `PINT` needs some information about the pulsar. In addition to the initial parameters of table 1, the parameters in table 2 are added.

Note that once the transformation is performed, the TOAs are as observed from the SSB, not in the frame of the pulsar. My implementation of these corrections using `PINT` can be found in appendix B.

Parallax	$0.59 \pm 2.000 \times 10^{-2}$ milliarcseconds (mas)	Observing frequency	407.5 MHz
Proper motion in RA	$16.97 \pm 3.000 \times 10^{-2}$ mas year^{-1}	Proper motion in DEC	$-10.37 \pm 5.000 \times 10^{-2}$ mas year^{-1}

Table 2: The extra parameters that must be input in `PINT` for pulsar timing. Taken from the ATNF Pulsar Catalogue, which collected the data from Deller et al. [2018].

4.3.2 Fitting

I keep only observations that have a high enough folded SNR to be accurate. I chose a SNR cutoff of 3.75, which was the lowest (to 0.05) which removed outliers. This is close to the previous analysis' SNR cutoff of 4, so comparisons can still be made.

There can be large differences between the observed TOAs and the timing model from tables 1 and 2. These are the pre-fit residuals. I use `PINT` to perform a least-squares fit of the frequency, frequency deceleration and position of the pulsar on the TOAs. The other parameters (with error) are fixed. After performing the fit and updating the model, the residuals of expected (updated model) TOA to observed TOA are as seen in figure 9.

Post-fit residuals can be a valuable source of information, that shows departure from a simple model by the pulsar itself. This can be due to planets, a binary companion, internal structure changes, etc. Sometimes, the processes are unknown. The residuals' evolution is called 'timing noise'.

Published residuals from the Jodrell Bank observatory are shown in figure 11. The last dip and rise in residuals on this graph matches the previous analysis' TOAs that go further in the past, in figure 10 – this is real timing noise due to pulsar processes. My TOAs have been taken over a shorter period, of linear increase of several milliseconds in timing residuals. This slope has been completely absorbed in the model. The timing model generated is not wrong, though - pre-fit timing residuals for this project actually decrease linearly with time from 25 to -30 ms. This is much larger than intrinsic pulsar timing noise, so the latter does not affect the new model much. The only way to recover timing noise with this routine is to run it on more observations!

The new fitted model can now be fed into the folding procedure, described in 4.1.3. This allows a much better estimation of the phase. To do so, command 2 is ran again with the `-absphase` option, and the `PINT` post-fit parameters. An updated model fold is shown in figure 12. At this point, the pulsar frequency and position parameters used in the pipeline are entirely derived from our observations!

4.4 Total pulse profile

With each pulse profile now folded accurately in phase (with a timing model refined thanks to our observations), they can be simply added together in phase and weighted to create a total pulse profile. This is an average pulse profile over a year of observations, which is a stable and unique pulsar identifier, as mentioned in 2.4).

`PRESTO` does not yet support adding weighted pulse profiles in absolute phase. I implemented it (in Appendix B) by adding them, weighted by their folded SNR. This weighting method is the same as `PSRCHIVE`'s [Hotan et al., 2004].

PRESTO only allows adding profiles using their TOA as the alignment, and the weights are computed by setting the off-pulse region's RMS equal for all profiles. Aligning the folds in absolute phase using an updated timing model is more precise than using their TOA. Indeed, the TOAs collectively tend towards the new model, but each has a rather large error: it is better to consider them as an ensemble rather than individually.

The final summed pulse profile is shown in figure 13; it has the same SNR cutoff as the TOAs, 3.75.

When I tested the analysis on raw data (no cleaning), the total pulse profile had much greater residuals and lost most of its shape. The previous total pulse profile, implemented by a MATLAB script, used the maximum of the profiles for alignment (less precise than a timing model), and a SNR weight. The residuals to the template were also greater than mine, they are seen in figure 14.

4.5 Pulsar parameters evaluation

The `PINT` timing fit in section 4.3 yielded the following results[1], that can be compared with table 1:

- $f = 1.39954153774 \pm 9.7 \times 10^{-10}$ Hz , which is in agreement with the value from Hobbs et al. [2004], with a two orders of magnitude greater error (their observations span many years);
- $\dot{f} = -4.00890 \times 10^{-15} \pm 9.6 \times 10^{-19}$ Hz s^{-1} , which is not quite within the accepted error bounds of Hobbs et al. [2004], but very near ($\simeq 2 \times 10^{-18}$ Hz s^{-1} away), with an error one order of magnitude greater;

[1]The results have been truncated to their error precision and errors rounded to two significant figures, as customary. The updated model contains more significant figures that are used in the second fold in absolute phase.

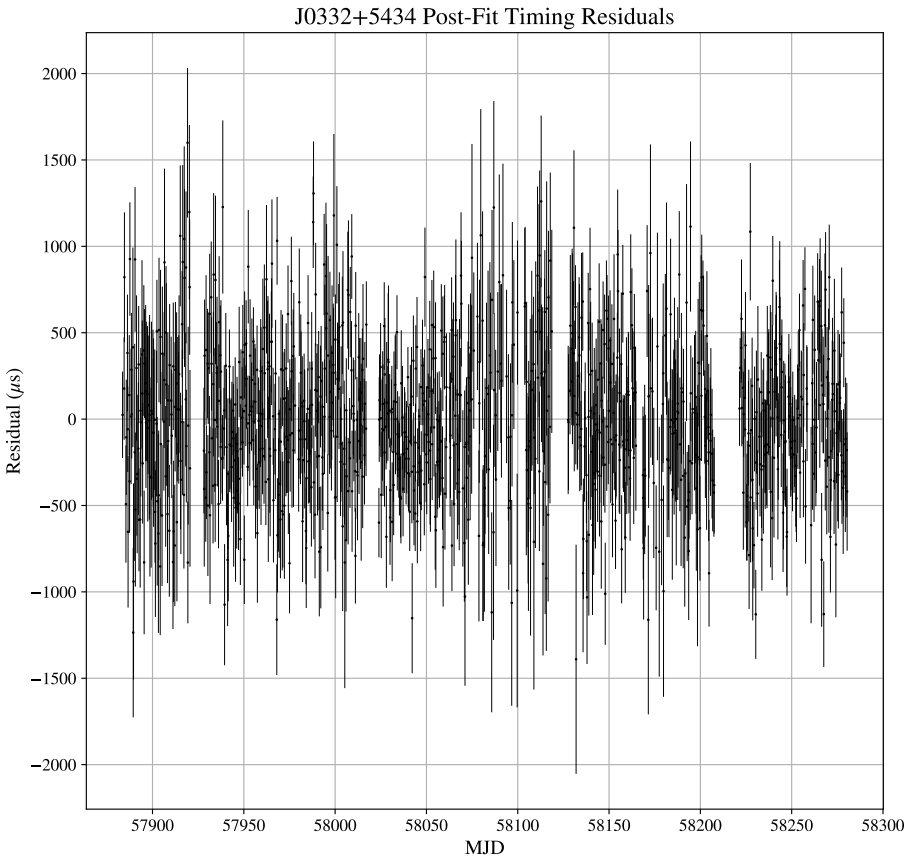

Figure 9: The post-fit residuals generated by `PINT`. There are no visible trends. Most of the residuals are within 1000 μs (1 ms) of the model. An increasing linear trend of a few milliseconds in timing noise has been completely absorbed by the timing model.

- Right Ascension = 03:32:59.36004193$\pm$3.9$\times10^{-7}$ deg and Declination = 54:34:43.2890116$\pm$8.3$\times10^{-6}$ deg. This is not taken at the same epoch as the model position [Deller et al., 2018]. It is very interesting to see how precisely the position of the pulsar can be determined using solely the Doppler effect from the Earth's rotations!

From there, I determine the characteristic age τ and characteristic magnetic field B (lower limit at the surface) of PSR J0332+5434 [Condon and Ransom, 2016, Chapter 6], which are standard quantities in pulsar astronomy (precision is not necessary as these are approximations):

$$B = 3.2 \times 10^{19} \sqrt{\frac{-\dot{f}}{f^3}} \simeq 1.22 \times 10^{12}\,\text{Gauss} \tag{8}$$

$$\tau = \frac{f}{-2\dot{f}} \simeq 5.53\,\text{million years} \tag{9}$$

These values are consistent with the ATNF Pulsar Catalogue's, which have been derived from the frequency values in table 1.

5 Discussion

Throughout this analysis, some steps could have been improved:

- In data cleaning (section 3.2.2), using a median filter with a sliding window rather than over data blocks (long computing time);

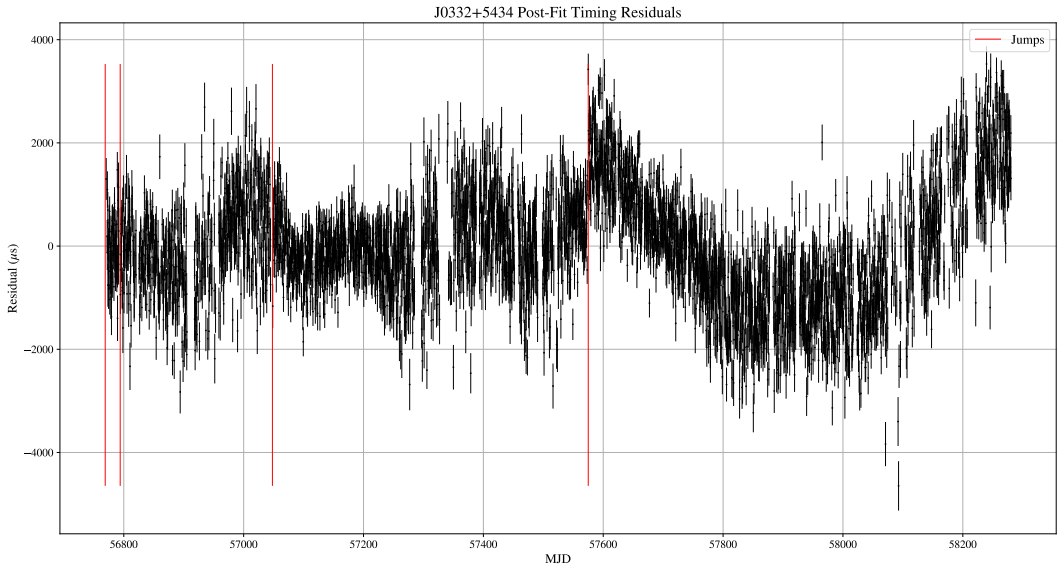

Figure 10: The `PINT` post-fit residuals from the TOAs of the previous MATLAB pipeline (not this project's). There are several trends due to the pulsar, and jumps (plotted) from hardware/software changes. This dataset spans March 2014 to June 2018. The observations used in this project span the last linear increase on this graph (May 2017 to June 2018). The dip and rise starting just after the last jump match the published PSR J0332+5434 residuals, shown in 11. This is real timing noise, originating from pulsar processes that depart from a simple model. In the previous version of this analysis, the timing and fitting was done with `TEMPO2`, which is equivalent. Note that I encountered a jump fitting bug in `PINT`, which was fixed by Dr. Jing Luo when I raised the issue.

- When matching the template pulse profile for TOA finding in section 4.2.1, using Gaussian Interpolation Shift rather than `FFTFIT`, since it is more adapted for low-SNR pulse profiles (not implemented in `PRESTO`, but in `PSRCHIVE`);
- In TOA finding again, using the real template rather than a Gaussian approximation (again, not possible in `PRESTO`, but available in `PSRCHIVE`);
- Overall, using more observations to uncover timing noise (for example, re-cleaning the previously cleaned observations that are the only data available before May 2017).

Some further research is also possible:

- Studying the variation in brightness of the pulses and compare with literature, e.g. Esamdin et al. [2004]. This may be difficult due to our low SNR, but it can be implemented with `PSRCHIVE`.
- A Bayesian analysis of the time PSR J0332+5434 spends in normal and abnormal mode (see figure 13, and section 2.4).

6 Conclusion

The aim of this project was to upgrade the data analysis pipeline of the Acre Road pulsar telescope to current research standards. The year of observations used in this project, made with an array of four Yagi antennae with $10\,\mathrm{m}^2$ effective area, a 13 degree beam and a microsecond precision clock, are of a much lower quality than usual pulsar astronomy. To recover the pulsar signal from below noise levels, I applied stringent data cleaning, and folded the 4-hour observations in phase with `PRESTO`, taking into account pulse frequency variations using `TEMPO`. I obtained pulse times of arrival using the `FFTFIT` method in `PRESTO` with a four-component Gaussian template of PSR J0332+5434's pulse shape. I then performed a relativistic frame transformation of the observed topocentric pulses to the Solar System Barycenter in `PINT`. I thus least-squares fitted the pulsar frequency, frequency derivative and position; and refined my analysis with these new parameters. Finally, I computed a total summed pulse profile of the year of observations.

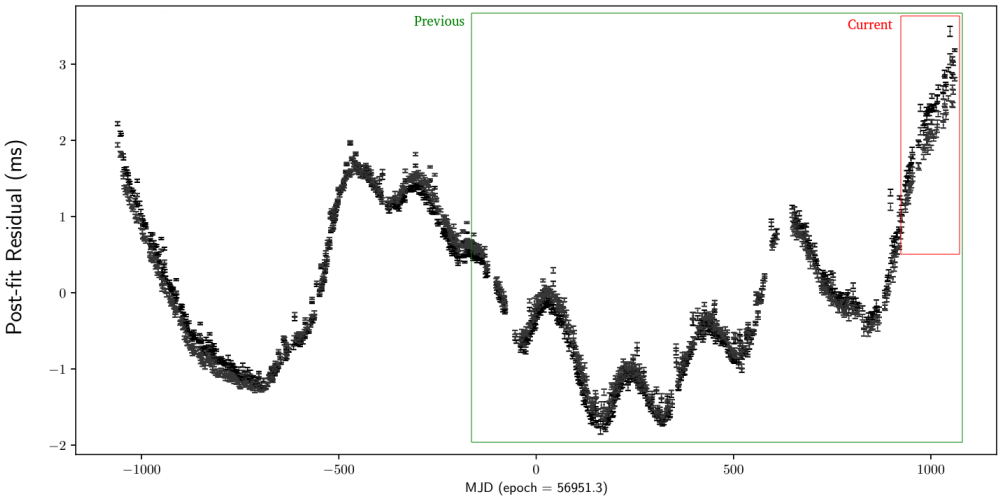

Figure 11: PSR J0332+5434's post-fit residuals adapted from Kwofie [2018]. Like the template, these observations were made by the Jodrell Bank observatory, in England, but using the 12m telescope at 610MHz. The green box encloses approximately the observation span of the previous pipeline's residuals (figure 10), while the red is for this project's (figure 9). This graph spans January 2012 to July 2017, and thus only a few months are visible for this analysis. These were the most recent published observations I could find. A linear increase in timing noise is apparent in this project's timeframe.

The project has largely succeeded in its aim of superseding the previous pipeline, through the use of research software. Indeed, the observations are cleaner, and folded much more accurately. Overall, TOAs have a smaller error bar and folded pulse profiles a larger SNR. The smallest error bar is 173.95 μs, which is very precise considering the quality of the observations, and the largest folded SNR is 13.48. The total pulse profile is very close to the Jodrell Bank template, and has smaller residuals than the previous method's. I further determined the pulsar's frequency parameters and position accurately and with great precision. The inferred age and magnetic field agree with published values.

References

Dipankar Bhattacharya. Detection of Radio Emission from Pulsars. In *The Many Faces of Neutron Stars*, pages 103–128. Springer Netherlands, Dordrecht, 1998. ISBN 0792351940.

T. W. Cole and J. D.H. Pilkington. Search for pulsating radio sources in the declination range + 44° to + 90°. *Nature*, 219(5154):574–576, 1968. URL www.doi.org/10.1038/219574a0.

James Condon and Scott Ransom. *Essential Radio Astronomy*. Princeton University Press, 2016. ISBN 978-0-691-13779-7. URL www.cv.nrao.edu/~sransom/web/xxx.html.

A. T. Deller, W. M. Goss, W. F. Brisken, S. Chatterjee, J. M. Cordes, G. H. Janssen, Y. Y. Kovalev, T. J. W. Lazio, L. Petrov, B. W. Stappers, and A. Lyne. Microarcsecond VLBI pulsar astrometry with PSRPI II. parallax distances for 57 pulsars. *The Astrophysical Journal*, 875(2):100, 2018. URL www.dx.doi.org/10.3847/1538-4357/ab11c7.

R T Edwards, G B Hobbs, and R N Manchester. TEMPO2, a new pulsar timing package - II. The timing model and precision estimates. *Monthly Notices of the Royal Astronomical Society*, 372(4):1549–1574, 11 2006. URL www.dx.doi.org/10.1111/j.1365-2966.2006.10870.x.

A. Esamdin, A. Z. Zhou, and X. J. Wu. A study of the long-term flux density variation of PSRs B0329+54 and B1508+55. *Astronomy & Astrophysics*, 425(3):949–954, 10 2004. URL www.doi.org/10.1051/0004-6361:20040490.

Ettus Research. USRP B200 SDR Kit - Single Channel Transceiver (70 MHz - 6GHz). URL www.ettus.com/all-products/ub200-kit/.

GNURadio. The free and open software radio ecosystem. URL www.gnuradio.org.

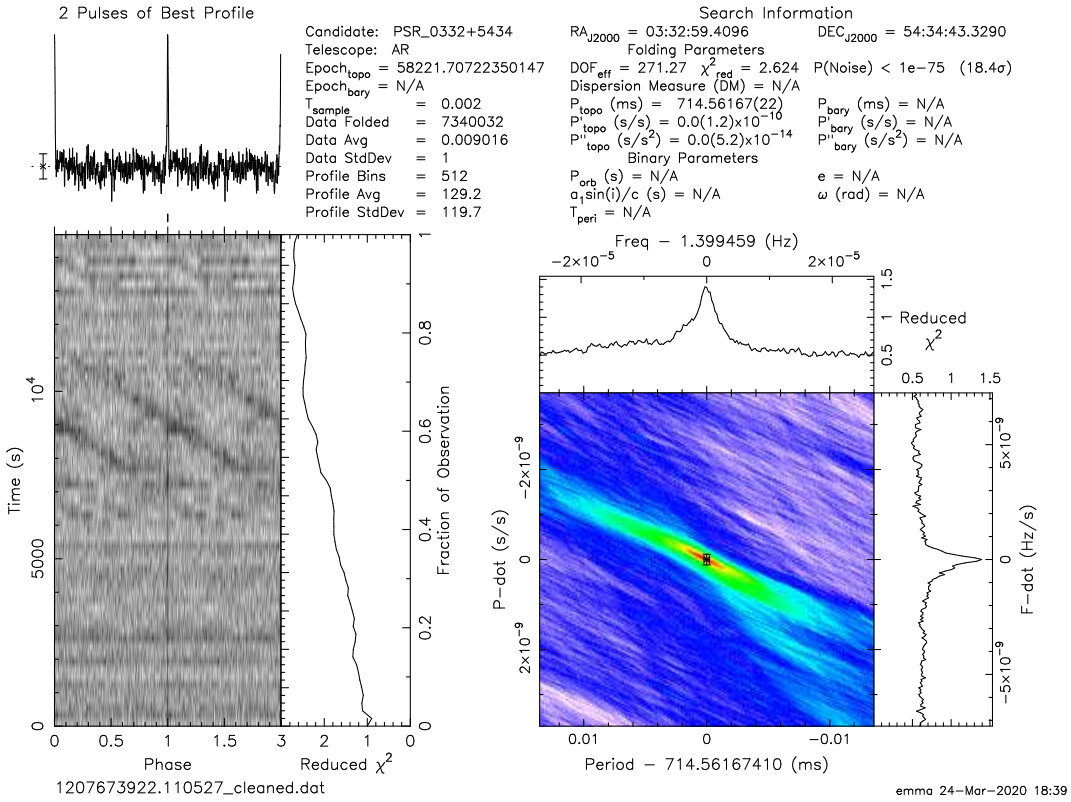

Figure 12: The best fold output of the year of observations, with a SNR of 13.36 and a TOA error bar of 173.51 μs. In the top left corner appears the summed folded pulse profile of this 4-hour observation. Here, the summed pulse is bright, sharp, and well above the noise levels. Below this folded pulse profile, the data timeseries is shown in a waterfall plot, with each horizontal line of observed power lasting exactly one rotation. The observed pulses appear as a faint vertical line at phase 1. Some noise is visible on the waterfall plot. Transient noise appears as a horizontal line near the beginning of the observation. Later, periodic noise appears as slant lines. If I was folding at the frequency of this noise, these would appear as a straight line. This highlights the importance of correct folding to avoid summing phase drifts and widening the pulse [Lorimer and Kramer, 2005, pp. 168-169]. On the right, a grid of frequencies and frequency derivatives present in the dataset is shown, with clear peaks at PSR J0332+5434's values. This parameter space is **not** searched. Rather, the pulsar parameters (shown above the grid among some folding results) are input with the polynomial coefficients. This means that even if noise frequencies are dominant, the frequency shown will stay in the centre of the grid. The aim of folding here is not to find the frequency of the pulsar, but to produce an accurately summed pulse.

T. Gold. Rotating neutron stars as the origin of the pulsating radio sources. *Nature*, 218:731–732, 1968. URL www.doi.org/10.1038/218731a0.

P. Goldreich and W. EL Julian. Pulsar Electrodynamics. *The Astrophysical Journal*, 157(August):9, 1969. URL www.doi.org/10.1086/150119.

D. M. Gould and A. G. Lyne. Multifrequency polarimetry of 300 radio pulsars. *Monthly Notices of the Royal Astronomical Society*, 301(1):235–260, 11 1998. URL www.doi.org/10.1046/j.1365-8711.1998.02018.x.

T. H. Hankins. Microsecond Intensity Variations in the Radio Emissions from CP 0950. *The Astrophysical Journal*, 169:487, 11 1971. URL www.doi.org/10.1086/151164.

A. Hewish, S. J. Bell, J. D. H. Pilkington, P. F. Scott, and R. A. Collins. Observation of a Rapidly Pulsating Radio Source. *Nature*, 217(5130):709–713, 2 1968. URL www.doi.org/10.1038/217709a0.

G Hobbs, A Lyne, and M Kramer. Long-term Timing of 374 Pulsars. *Symposium - International Astronomical Union*, 218:431–432, 2004. URL www.doi.org/10.1017/s0074180900181562.

G. Hobbs, R. Edwards, and R. Manchester. TEMPO2, a new pulsar timing package. I: Overview. (February), 3 2006. URL www.dx.doi.org/10.1111/j.1365-2966.2006.10302.x.

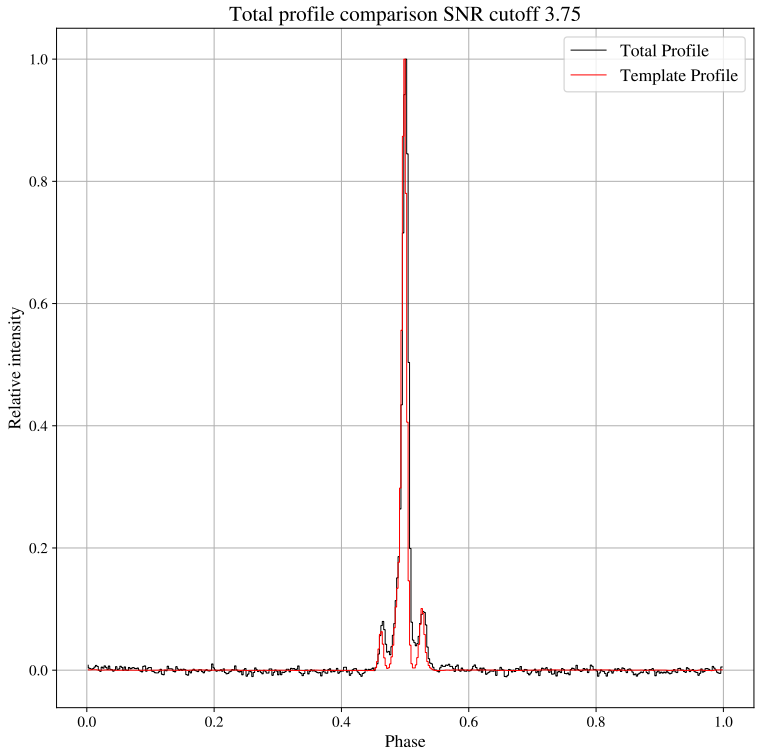

Figure 13: My total pulse profile. Comparing to Jodrell Bank's, there is some extra intensity in between the three peaks. This is probably due to our low SNR, which leads to wider peaks and less precision in alignment. Some off-pulse bins appear slightly correlated. This is a normal artefact from `PRESTO` due to the ratio of total pulse profile phase bin to time series bin (Scott Ransom, e-mail communication). The middle and right peak heights are a great match. The left peak, however, appears slightly more intense than the template's. This is completely normal. During the year of Acre Road observations, PSR J0332+5434 has spent some time in 'abnormal mode', i.e. the pulse shape average changes. In this non-dominant mode, the left peak is stronger [Kwofie, 2018, figure 4.1]. Jodrell Bank's template was integrated over one hour of observations, so it is plausible that the pulsar had not switched significantly then.

George Hobbs and Russell Edwards. TEMPO: Pulsar timing data analysis, 2012. URL www.ascl.net/1509.002.

A. W. Hotan, W. van Straten, and R. N. Manchester. PSRCHIVE and PSRFITS : An Open Approach to Radio Pulsar Data Storage and Analysis. *Publications of the Astronomical Society of Australia*, 21(3):302–309, 3 2004. URL www.doi.org/10.1071/AS04022.

A. W. Hotan, M. Bailes, and S. M. Ord. PSR J0737-3039A: baseband timing and polarimetry. *Monthly Notices of the Royal Astronomical Society*, 362(4):1267–1272, 8 2005. URL www.doi.org/10.1111/j.1365-2966.2005.09389.x.

Rudolf Kippenhahn, Alfred Weigert, and Achim Weiss. *Stellar Structure and Evolution*. Astronomy and Astrophysics Library. Springer Berlin Heidelberg, 2nd edition, 2012. ISBN 978-3-642-30255-8. URL www.doi.org/10.1007/978-3-642-30304-3.

Joseph A Kwofie. *Timing noise of PSR B0329+054 and its frequent mode changing*. PhD thesis, University of Manchester, 2018. URL www.research.manchester.ac.uk/portal/en/theses/timing-noise-of-psr-b032954-and-its-frequent-mode-changing(5976f836-cfde-4d14-a8b8-c1cc409f7531).html.

Marcus D. Leech. simple_ra : Simple integrated radio astronomy receiver for GNU Radio. URL www.github.com/patchvonbraun/simple_ra.

D Lorimer. SIGPROC : Pulsar Signal Processing Program, 2011. URL www.ascl.net/1107.016.

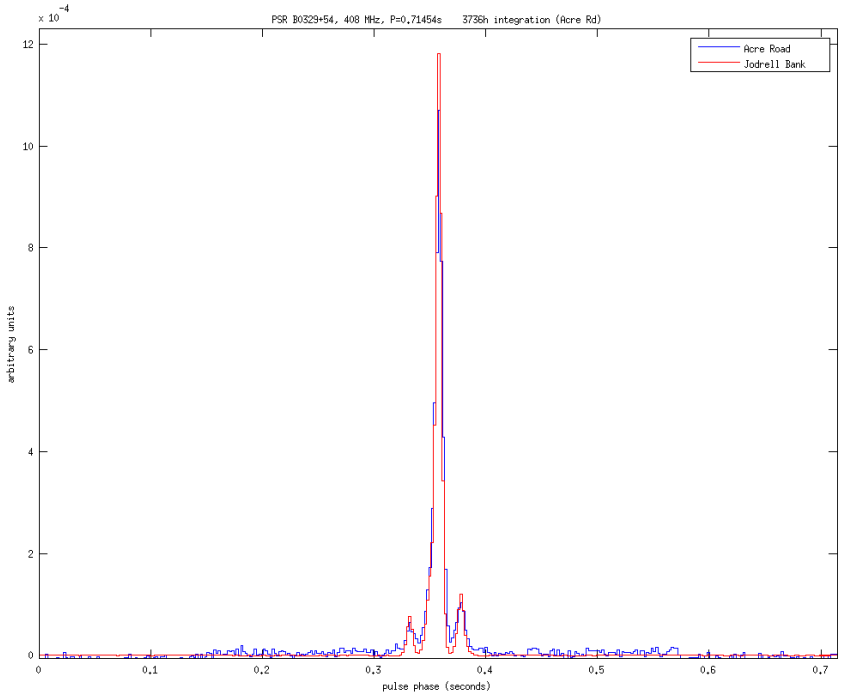

Figure 14: The previous analysis' total pulse profile. The middle peak's height does not match the template, while the side peaks do. The modes averaged over four years are closer to the Jodrell Bank template. There are extra residuals up to 0.2 in phase away from the pulse, which are not present in my total pulse profile. There is some extra intensity between peaks again.

D. R. Lorimer and M. Kramer. *Handbook of pulsar astronomy*. Cambridge University Press, 2005. ISBN 9780521828239.

Jing Luo, Scott Ransom, Paul Demorest, Rutger van Haasteren, Paul Ray, Kevin Stovall, Matteo Bachetti, Anne Archibald, Matthew Kerr, Jonathan Colen, and Fredric Jenet. PINT: PINT is Not TEMPO3. 2019. URL www.ascl.net/1902.007.

A. Lyne and F. Graham-Smith. *Pulsar Astronomy*. Cambridge University Press, 2012. URL www.doi.org/10.1017/CBO9780511844584.

R N Manchester, G. B. Hobbs, A Teoh, and M Hobbs. The Australia Telescope National Facility Pulsar Catalogue. *The Astronomical Journal*, 129(4):1993–2006, 4 2005. URL www.doi.org/10.1086/428488.

Michael Perreur-Loyd. Pulsar Monitoring Antenna Design Project, 2003. URL www.physics.gla.ac.uk/~mplloyd/Glasgow/Radiotelescope/RTpage1.html.

Scott Ransom. PRESTO: PulsaR Exploration and Search TOolkit, 2011. URL www.ascl.net/1107.017.

I. H. Stairs. Pulsar Observations II. – Coherent Dedispersion Polarimetry, and Timing. In *ASP Conference Proceedings*, volume 278, pages 251–269, 2002. URL http://www.aspbooks.org/a/volumes/article_details/?paper_id=25613.

J. H. Taylor. Pulsar timing and relativistic gravity. *Classical and Quantum Gravity*, 10(S):S167–S174, 12 1993. URL www.doi.org/10.1088/0264-9381/10/S/017.

Trimble. Thunderbolt® E GPS Disciplined Clock. URL www.trimble.com/Timing/thunderbolt-e.aspx.

W. van Straten and M. Bailes. DSPSR: Digital Signal Processing Software for Pulsar Astronomy. *Publications of the Astronomical Society of Australia*, 28(1):1–14, 8 2010. URL www.dx.doi.org/10.1071/AS10021.

Graham Woan. *The Cambridge Handbook of Physics Formulas*. Cambridge University Press, 6 2000. ISBN 9780521575072. URL www.doi.org/10.1017/CBO9780511755828.

A Acknowledgements

I thank my supervisor, Pr. Graham Woan, for passing on the pulsar fever. I am to continue working on them for my PhD. Thank you for the many hours spent teaching and kindly helping me in the past few years. I also thank the `PINT` and `PRESTO` team, specifically Prof. Scott Ransom, Dr. Paul Ray, Dr. Jing Luo and Camryn Phillips for their help and the software fixes/additions.

B Software

See the iPython notebook on my GitHub page.